HOKKAIDO UNIVERSITY

Title	Detailed simulation of morphodynamics: 3. Ripples and dunes
Author(s)	Nabi, Mohamed; de Vriend, H. J.; Mosselman, E. et al.
Citation	Water resources research, 49(9), 5930-5943 https://doi.org/10.1002/wrcr.20457
Issue Date	2013-09
Doc URL	https://hdl.handle.net/2115/56455
Rights	Copyright 2013 American Geophysical Union.
Type	journal article
File Information	wrcr20457.pdf

Hokkaido University Collection of Scholarly and Academic Papers : HUSCAP

WATER RESOURCES RESEARCH, VOL. 49, 5930–5943, doi:10.1002/wrcr.20457, 2013

Detailed simulation of morphodynamics: 3. Ripples and dunes

M. Nabi,[1] H. J. de Vriend,[2,3] E. Mosselman,[2,3] C. J. Sloff,[2,3] and Y. Shimizu[1]

Received 27 January 2012; revised 1 August 2013; accepted 2 August 2013; published 20 September 2013.

[1] We present a 3-D physics-based high-resolution modeling approach to the dynamics of underwater ripples and dunes. The flow is modeled by large eddy simulation on a Cartesian grid with local refinements. The sediment transport is modeled by computing pickup, transport over the bed, transport in the water column, and deposition of rigid spherical particles in a Lagrangian framework. The morphological development of the bed is modeled by a sediment balance equation in which the pickup and deposition from the sediment motion submodels appear as source and sink terms. The model realistically replicated the formation and migration of dunes. Model results showed a good agreement with data from five flume experiments. We subsequently applied the model to investigate the effect of sediment grain size on ripples. Finer sediments were found to yield more superimposed ripples than coarser sediments. Moreover, under the same hydrodynamic conditions, the finer sediments yielded two-dimensional bed forms, whereas for coarser sediment irregularities increased. We extended the tests to pronounced 3-D morphologies by simulating the development of local scour at a pier. The results agreed well with experimental data. The model contributes to unraveling the complex problem of small-scale morphodynamics and may be used in a wide range of applications, for instance, to develop more reliable parameterizations of small-scale processes for application in large-scale morphodynamic models.

Citation: Nabi, M., H. J. de Vriend, E. Mosselman, C. J. Sloff, and Y. Shimizu (2013), Detailed simulation of morphodynamics: 3. Ripples and dunes, *Water Resour. Res.*, *49*, 5930–5943, doi:10.1002/wrcr.20457.

1. Introduction

[2] Ripples and dunes are alluvial river bed forms on the smallest scales of fluvial morphodynamics. For flows of increasing strength, a typical sequence of bed forms occurs: lower flat bed → ripples → dunes → upper flat bed → antidunes → pools and chutes [*Simons et al.*, 1961; *Guy et al.*, 1966; *Simons and Richardson*, 1966]. Features up to and including dunes are generally termed lower-flow-regime bed forms, characterized by a low bed-material transport rate and a relatively high flow resistance.

[3] Early studies of river bed forms were based on results from flume experiments. Those studies attempted to use mean flow and sediment properties to indicate what bed forms are to be expected under which conditions, and to derive parameterized prediction formulae for bed form geometries, called roughness predictors. *Kennedy* [1963] is considered to be the first to analyze the formation and the geometry of wave-like phenomena on mobile sand beds. His model was based on a two-dimensional potential flow over an erodible bed. To produce an unstable wave, he related the local sediment transport rate to the local fluid velocity, with a lag distance between sediment transport and flow velocity. *Engelund* [1970] investigated the stability of a sand bed by a two-dimensional mathematical model based on the vorticity transport equation. The model takes account of the internal friction and describes the nonuniform distribution of the suspended sediment. The inclusion of the fluid friction and a model of the sediment transport mechanism leads to bed forms rather different from those obtained by potential flow analysis. *Richards* [1980] added viscous effects to the flow model, including a one-dimensional turbulence model for flow over a hydrodynamically rough bed, to study the formation of ripples and dunes. His results showed that ripple formation is independent of the flow depth. *Sumer and Bakioglu* [1984] extended this work to hydrodynamically smooth flows to analyze ripple formation.

[4] Both two-dimensional and three-dimensional dunes are observed in nature and laboratory experiments [*Venditti*, 2007]. Two-dimensional ripples and dunes are fairly regular in their spacing, height, and length. Their crest lines are straight or weakly sinuous and are oriented perpendicular to the flow. Contrastingly, 3-D features are more irregular in spacing, height, and length, with highly sinuous or discontinuous crest lines [*Ashley*, 1990]. *Southard and Boguchwal* [1990] provide a plotting methodology and extensive bed form phase diagrams, showing the occurrence of ripples, dunes, antidunes, or plane bed for different

Companion paper to *Nabi et al.* [2012] doi:10.1029/2012WR011911 and *Nabi et al.* [2013] doi:10.1002/wrcr.20303.

[1]Laboratory of Hydraulic Research, Graduate School of Engineering, Hokkaido University, Sapporo, Japan.
[2]Section of Hydraulic Engineering, Delft University of Technology, Delft, Netherlands.
[3]Deltares, Delft, Netherlands.

Corresponding author: M. Nabi, Laboratory of Hydraulic Research, Graduate School of Engineering, Hokkaido University, Sapporo, 060–8628, Japan. (m.nabi@eng.hokudai.ac.jp)

©2013. American Geophysical Union. All Rights Reserved.
0043-1397/13/10.1002/wrcr.20457

sediment and flow properties. The formation and development of these bed forms are associated with local hydrodynamic and sediment transport characteristics, as well as with the flow-induced forces on the bed, which in turn are influenced by the bed forms. Few attempts have been made so far to study the generation, migration, splitting, merging, and superimposition of dunes under constant or variable discharges [*Wilbers*, 2004; *Venditti et al*., 2005]. These phenomena are still not fully understood and difficult to study in the field or even in the laboratory.

[5] Recently, significant progress has been made in understanding bed form dynamics, thanks to significant advances in the ability to monitor flow and bed form morphology in laboratory and field [*Venditti et al*., 2005; *Tuijnder et al*., 2009], as well as in its numerical modeling [*Giri and Shimizu*, 2006; *Shimizu et al*., 2009; *Niemann et al*., 2011]. Nowadays, numerical modeling captures not only the characteristics of the mean flow field but also those of turbulence, including coherent flow structures above nonflat beds [*Kraft et al*., 2011; *Nabi et al*., 2012b]. These advances of numerical modeling bring us into a position to make radical progress in quantifying, modeling, and understanding the dynamics and kinematics of alluvial bed forms [*Best*, 2005]. Thanks to the increased computer power and novel numerical techniques, detailed descriptions of turbulent flow and sediment motion can be used for process-based simulation of ripples and dunes. The local flow field is determined from well-established high-resolution hydrodynamic modeling concepts like direct numerical simulation (DNS), large eddy simulation (LES), and unsteady Reynolds-averaged Navier-Stokes turbulence closure (URANS). The description of the local and instantaneous sediment motion incorporated in these models is equally important but much less well established (see the companion paper *Nabi et al*. [2013]).

[6] Several researchers have applied numerical methods to simulate the flow over fixed ripples, in order to understand the effects of bed forms on the flow field and the implications for the sediment transport. *Zedler and Street* [2001], for instance, focused on the initial entrainment and transport of suspended sediment in flows over fixed ripples. A well-resolved large eddy simulation (LES) was employed to examine in some detail the role and effect of coherent structures that occur near the bed.

[7] None of the existing numerical models is capable of simulating the generation and migration of dunes in an entirely physics-based way. Yet, numerical models were used to address these issues. *Fredsøe* [1982] proposed a model in which the dune height was determined by assuming the dune to move as a migrating front. The length of the dune was determined using a semiempirical flow description. *Tjerry and Fredsøe* [2005] refined the Fredsøe model by describing the flow with a numerical flow model based on a two-equation turbulence closure. They were able to explain how the streamline curvature above the mildly sloping upstream part of the dune influences the dune length. The dune height, however, was not explained by this model; hence, the earlier results from *Fredsøe* [1982] were employed.

[8] *Giri and Shimizu* [2006] proposed a (vertically) two-dimensional morphodynamic model that successfully reproduces fluid and bed form dynamics in a coupled manner under steady flows. They described turbulence with a nonlinear $k-\epsilon$ model. A nonequilibrium sediment transport approach, treating pickup and deposition of sediment empirically, was used along with an assumed mean sediment particle step length. Despite its attractive features, the shape of the dunes is strongly dependent on the definition of the particle step length, which is unknown. Hence, this model cannot always predict the shape of the dunes correctly. Furthermore, this model uses a URANS turbulence closure, which removes the turbulent fluctuations. Hence, it removes the shear stress fluctuations and their effects on the sediment pickup. The stress fluctuations are an important element in the formation of ripples on the stoss sides of the dunes, which cannot be simulated by RANS or URANS approaches (resulting in smooth dunes).

[9] *Paarlberg et al*. [2009] developed a two-dimensional vertical model assuming hydrostatic pressure conditions. The sediment transport was computed using a Meyer-Peter-Müller type of equation, including gravitational bed slope effects and a critical bed shear stress. The flow model was simplified by parameterization of the flow in the recirculation zone and by considering the separation streamline as an artificial bed. This model successfully simulated the bed form evolution from a flat bed, with initial perturbations. However, in this model, dunes keep merging until one dune covers the full domain, which is unrealistic. Moreover, bed load sediment transport is evaluated using the turbulence-averaged bed shear stress as flow parameter, which is not accurate in case of nonuniform flow with developing boundary layers associated with significant spatial variations in turbulence structures [*Nelson et al*., 1995].

[10] An interesting study on numerical modeling of dune dynamics was presented by *Niemann et al*. [2011]. Their hydrodynamic model is based on a $k-\omega$ turbulence closure and the transport model is based on a conventional bed-load transport formula (Meyer-Peter and Müller), but including a slope effect and an avalanche model to stabilize the slope of the lee face. The model is found to be capable of predicting the dune evolution from an initial perturbation. The model uses a filter to smoothen the bed form. *Niemann et al*. [2011] argue that the filter locally "rearranges" the sediment on the bed to some extent and that its effect can thus be interpreted as "artificial" erosion or deposition.

[11] *Kraft et al*. [2011] simulated the sediment transport in a turbulent channel flow over the sediment bed with a ripple structure by means of a large eddy simulation. The distribution of the suspended sediment concentration is calculated with the convection-diffusion equation. The rate of sedimentation depends on the concentration near the bed and the settling velocity of the sediment. The migration and deformation of the interface between the sediment bed and the fluid flow is captured by the level-set method. A global effect of these local processes is the migration of two-dimensional ripples. However, the migration of the ripples is relatively small and the bed starts its motion from prior initialized ripples. The migration of the ripples is not sufficiently significant for practical applications.

[12] The detailed modeling approaches, mentioned above, are all two-dimensional, but the nature of flow over three-dimensional dunes is very different from that in two dimensions, to the extent that the application of 2-D models to field situations requires careful attention [*Best*, 2005].

Field observations suggest that 3-D models are necessary to describe natural bed forms.

[13] It is against this background that we developed a high-resolution 3-D numerical model for morphodynamic processes on small temporal and spatial scales, based on large eddy simulation, particle-based transport of sediment, and adaptive grid refinement and immersed-boundary techniques for mobile sediment beds. The flow and sediment transport submodels are presented in two companion papers by *Nabi et al*. [2012b, 2013]. The flow model (part I) simulates the detailed hydrodynamics by large eddy simulation on a multilevel (i.e., locally refined) Cartesian grid. In the sediment transport model (part II), the sediment grains are considered as spherical particles moving with the fluid (in a Lagrangian framework). A discrete-element model is developed for sediment pickup from the bed, movement of particles along the bed and in the water column, and deposition on the bed. In the present paper (part III), we focus on the formation and development of ripples and dunes, presenting the first fully process-based 3-D model for the simulation of bed form evolution and migration. This model gives a better insight into the generation and migration of ripples and dunes and clarifies the effect of coherent turbulence structures on the development of the bed features. The novelty of the model is also its physics-based prediction of the bed forms for relatively long temporal scales (experimental scale) within reasonable computational times. We verify the model on four flume experiments by *Bakker et al*. [1986] and one flume experiment by *Crosato et al*. [2011]. Subsequently, we use the settings for the experiment by *Crosato et al*. [2011] to investigate the effect of sediment grain size on ripples and dunes. Finally, we extend the verification to pronounced 3-D morphologies by simulating the experiments by *Khosronejad et al*. [2012] on the development of local scour at a pier.

2. Numerical Model

2.1. Overview

[14] The 3-D large eddy simulation model proposed by *Nabi et al*. [2012b] is employed for the hydrodynamics. This model uses a multilevel Cartesian grid, on which the governing equations are discretized using a staggered-grid approach and their solution is advanced in time using a fractional-step method. Wherever necessary, automatic local grid refinement and adaptation to the bed topography is applied. A ghost-cell immersed-boundary technique is implemented for the cells which intersect the immersed boundaries. The momentum equations are discretized with a finite-volume method and are solved with the Adams-Bashforth-Cranck-Nicholson method to avoid the necessity of small Courant numbers. Large eddy simulation is applied for turbulence. This model is capable of performing well for problems with relatively large temporal scales such as alluvial processes.

[15] A sophisticated sediment model based on particle movement in a Lagrangian field proposed by *Nabi et al*. [2013] is employed. This model includes four submodels, namely, sediment pickup, transport over the bed (bed load without saltation), transport in the water column (saltation and suspended load), and deposition. These submodels are combined to form the total motion of sediment under the turbulent flows.

[16] The computation of morphodynamic changes is based on the sediment balance equation; with the sediment pickup and deposition obtained from the sediment model as source and sink terms. In the next sections, the morphodynamic model based on particle motion is discussed in more detail.

2.2. Morphodynamic Model

[17] To avoid the limitations of the existing models [*Giri and Shimizu*, 2006; *Niemann et al*., 2011; *Paarlberg et al*., 2009; *Kraft et al*., 2011], a more physics-based model has been implemented, with the aim of obtaining a more realistic description of the evolution and migration of bed forms.

[18] The number of picked up and deposited particles is determined with the method proposed by *Nabi et al*. [2013]. In combination with a model for sediment transport over the bed, it is used to describe the evolution of the bed. The difference in the number of particles picked up and deposited for any portion of the bed indicates the amount of mass added to or taken away from that area. The change in bed level, Δz_{bed}, after time step Δt can be determined as

$$\Delta z_{bed} = \frac{A_2}{A_3}\frac{V_p\left(n_{depos} - n_{pickup}\right)}{S.C_{frac}} + \frac{\delta P_S}{\Delta x \Delta y} \tag{1}$$

and

$$z_{new} = z_{old} + \Delta z_{bed} \tag{2}$$

[19] The first and second terms in the right-hand side of equation (1) indicate the effect of sediment transport by pickup and deposition and by transport over the bed, respectively. z_{old} and z_{new} are the bed levels before and after deformation, S is the area from which the sediment is picked-up or to which the sediment is deposited, C_{frac} is the particle clustering factor, V_p is the volume of a single particle, n_{pickup} is the number of picked up particles, and n_{depos} is the number of deposited particles in time step Δt, which can be found according to *Nabi et al*. [2013] using Stokes number and particle diameter as criteria for deposition. Δx and Δy are the dimensions of the bed grid cells in streamwise and transverse directions, respectively. In the second term in the right-hand part of equation (1), $\delta P_S = P_{S,in} - P_{S,out}$ is the change in volumetric sediment transport for each cell associated with transport over the bed. Here $P_{S,in}$ denotes the sum of all sediment volumes transported over the bed into the control area from neighboring cells, and $P_{S,out}$ is the sum of all sediment volumes transported over the bed out of the control area to the neighboring cells. A_2 and A_3 are shape coefficients for spherical sand grains with two-dimensional and three-dimensional geometrical properties, namely $\pi/4$ and $\pi/6$, respectively. The submodel for sediment transport over the bed is discussed in more detail in *Nabi et al*. [2013].

2.3. Bed Geometry

[20] The bed is considered as a structured surface grid (Figure 1). The resolution of the grid for Δx and Δz is the same as the resolution of the finest computational grid that is attached to the bed. The bed level is defined in the center

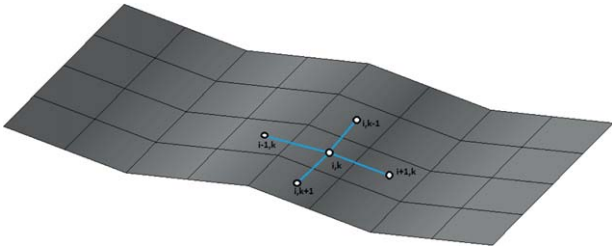

Figure 1. The bed is defined by a structured surface grid, and the bed level is located in the cell centers. The bed level at the face centers can be found by bilinear interpolation.

of each cell and can be interpolated to other points. Here bilinear interpolation is applied, which conserves second-order accuracy of the bed geometry. On the other hand, mass conservation has to be taken into account as the bed deforms. In case of periodic boundaries upstream and downstream, the sum of mass in the bed and mass of moving particles must be constant. If the boundaries are not periodic, sediment has to be fed upstream to compensate for the outflow through the downstream boundary.

3. Results

3.1. Comparison With Laboratory Experiments

[21] The formation and migration of ripples and dunes under turbulent flow conditions are presented in this section. A number of numerical tests were conducted to assess the capability of the proposed particle-based numerical model to simulate bed form evolution processes under steady discharges. The results are compared with a series of experiments conducted at Delft Hydraulics [*Bakker et al*., 1986].

[22] Forty experiments were carried out in a straight flume with constant discharge in the period of 1973–1980 [*Bakker et al*., 1986]. The length of the flume was 100 m with an adjustable width between 0.3 and 1.5 m. The discharge was varied between the experiments. The material used in these experiments consisted of uniform sand with $d_{50} = 0.78$ mm and density of 2660 kg/m^3. The sediment was supplied by means of a hydro-cyclone which discharged predefined amounts of sediment into the flume at regular intervals.

[23] We selected four experiments, referenced by T01, T11, T31, and T39 in *Bakker et al*. [1986]. Table 1 shows the corresponding experimental conditions. A part of the flume was simulated numerically by imposing periodic boundary conditions at the upstream and downstream ends of the model domain. This allowed using a relatively short domain length, so as to reduce the computational effort. A subset of the numerical runs has also been performed by *Shimizu et al*. [2009], to check the effect of the domain length. Using domain lengths of 1.6, 4, and 20 m, they found results from their model to be insensitive to domain length. Yet the domain length in our simulations covered several dune lengths, in order to minimize the effect of the periodic boundary conditions. The simulations indicated as RT01, RT11, RT31, and RT39 correspond to experiments T01, T11, T31, and T39, respectively. The domain length was chosen 5.1 m for RT01, 6 m for RT11, 4.7 m for RT31, and 4 m for RT39. Table 2 shows the conditions for the current simulations. Smooth solid boundary conditions in transverse direction were imposed, to account for the effect of the side walls in the experimental flume. In all simulations, a rigid-lid boundary condition was imposed at the water surface. *Niemann et al*. [2011] showed that a rigid-lid water surface condition has only minor effects on the bed forms as long as the Froude number is relatively low. The flow is driven by a pressure gradient, chosen such that in each time step, the discharge is kept constant. This means that the pressure gradient increases if the resistance increases because of dune growth. All simulations started from a flat bed without any initial perturbations.

Table 1. The Conditions for Four Experiments of *Bakker et al*. [1986] and for the Experiment of *Crosato et al*. [2011]

Experiment	Discharge (m^3/s)	Water Depth (m)	Flume Width (m)	Flow Velocity (m/s)
T01	0.151	0.197	1.500	0.511
T11	0.269	0.302	1.500	0.596
T31	0.116	0.208	1.125	0.495
T39	0.133	0.436	0.500	0.611
C01	0.007	0.045	0.600	0.252

Table 2. Conditions for the Simulated Cases

Experiment	Related Exp.	Domain Length (m)	$N_x \times N_y \times N_z$
RT01	T01	5.10	512 × 64 × 128
RT11	T11	6.00	512 × 64 × 128
RT31	T31	4.75	512 × 64 × 128
RT39	T39	4.00	512 × 128 × 64
RC01	C01	1.20	256 × 64 × 128

[24] In the first instance, the flow was simulated until it reached a steady state. Subsequently, the sediment transport and morphology models were started. The steady state of the flow was determined by monitoring the residuals of velocity and pressure, until they reached statistically constant values. For all simulations, a morphological factor of 20 was used, meaning that the time step in the morphological model equaled 20 times the time step in the flow model. Because of the small time steps and the slow change of the bed form, the associated error is negligible. In order to investigate the effect of the morphological factor, we simulated run RT39 with morphology factors of 5, 10, 20, and 30, and the results did not show a significant difference.

[25] Bed form dimensions were determined from the bed-level profile using a "zero-crossing" method [*Van der Mark et al*., 2008]. Length and height are defined by two successive intersections of the bed profile with the baseline. In 2-D situations, the baseline is the least squares straight line passing through the measured bed profile. The mean height and length of dunes are the averaged maximum height and the distance between two successive intersections, respectively. With this method, secondary bed forms (ripples migrating on the top of bed forms) can be identified, because the baseline may also intersect the small features on the bed. In previous studies, such secondary bed forms were often removed, as one was only interested in the mean dune dimensions. The effect of retaining

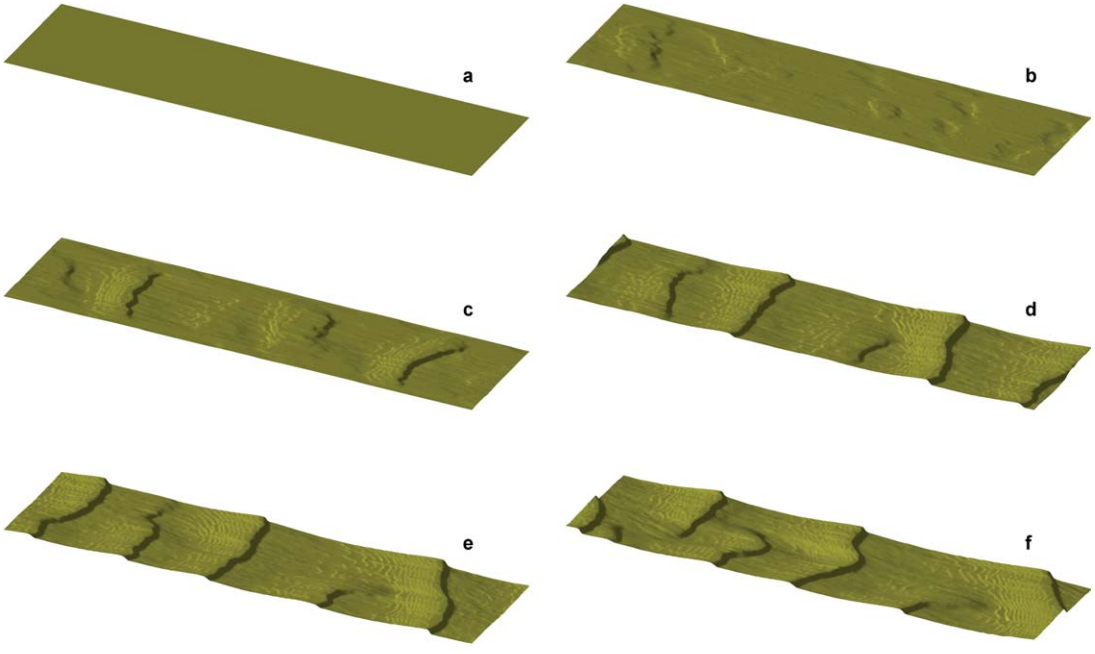

Figure 2. Bed form evolution simulated by numerical model for run RT11. (a) The bed begins from a flat bed, (b) later small deformations appear. (c) These deformations grow in size, and (d) the dunes begin to be formed. (e) Dunes migrate with closely two-dimensional features, and (f) finally three-dimensionality dominates.

secondary bed forms is that the mean dimensions of the bed forms will be somewhat smaller. The effect will be small, however, as the secondary bed forms will form on the crests of dunes, usually well above the mean bed level [*Tuijnder et al*., 2009].

[26] Figure 2 shows the generation and migration of dunes for run RT11. The bed evolved from flat to an equilibrium state, defined as a state in which the length and height of dunes remain statistically constant. Small deformations developed from the initially flat bed. These deformations grew and developed into dunes. In this simulation, the dunes migrated with closely two-dimensional features. Later on, the shape of the dunes changed to three-dimensional. The three-dimensional features of the bed can be observed in the computational results but only two-dimensional measurements are available from the experiments. Figure 3 shows the generation and migration of dunes for case RT39, in a narrow flume (0.5 m). In this case, the bed forms are much more two-dimensional. The bed forms began as ripples evolving into dunes that were small in length and height. Later on, these dunes merged and formed longer dunes. The height of these dunes grew until an equilibrium state was reached. An essential difference can be observed in the generation of dunes between cases RT11 and RT39. A comparison between Figures 2 and 3 shows that in case RT39 (narrow flume) the bed topography cannot deviate significantly from the two-dimensional form, as it is restricted by the side walls, whereas the bed form has a larger degree of freedom in case RT11.

[27] Figure 4 shows instantaneous snapshots of the bed forms for runs RT01 and RT31 after they reached their equilibrium. Simulations RT01 and RT31 show clearly three-dimensional features of dunes. In all simulations, ripples were generated on the stoss side of the dunes, which led to deformation of the dune profile. This phenomenon was already mentioned in *Best* [2005]. *Venditti et al*. [2005] define this structure as "sand sheets," without classifying these structures as ripples, dunes, or bars. The sheets formed downstream of the reattachment point at a distance that was invariant to the dune size. Dunes and sand sheets represent distinct scales of sediment transport with different migration rates [*Venditti et al*., 2005].

[28] Figure 5 shows the mean dune height evolution in time for all four simulations. The equilibrium dune height was found to be approximately 7.1, 7.7, 7, and 8.1 cm for runs RT01, RT11, RT31, and RT39, respectively. Figure 6 shows the evolution in time of the mean dune length. The equilibrium dune length was found to be approximately 1.3, 1.24, 1.39, and 1.33 m for runs RT01, RT11, RT31, and RT39, respectively. The experimental and numerical results for mean dune height and length in the equilibrium state are documented in Table 3. Moreover, the percentage of error between the experimental and the numerical results are given in this table. The simulated mean dune height and length agree well with the experimental measurement. However, an overprediction of 17% in the dune length for run RT31, and an under prediction of 12% in the dune height for run RT39 can be observed. The overprediction in length for run RT31 can be interpreted as the effect of three-dimensionality of dunes which cover the bed partially. Considering Figure 4 for run RT31 (right side), four dunes can be observed, but the second dune from the upstream direction does not cover the width of the domain completely. The nearly flat parts of the dune do not show up in the zero-crossing averaging approach and hence yield an overprediction of the mean length of dunes. It has to be mentioned that runs RT01 to RT39 were carried out under different flow conditions, yielding different bed form

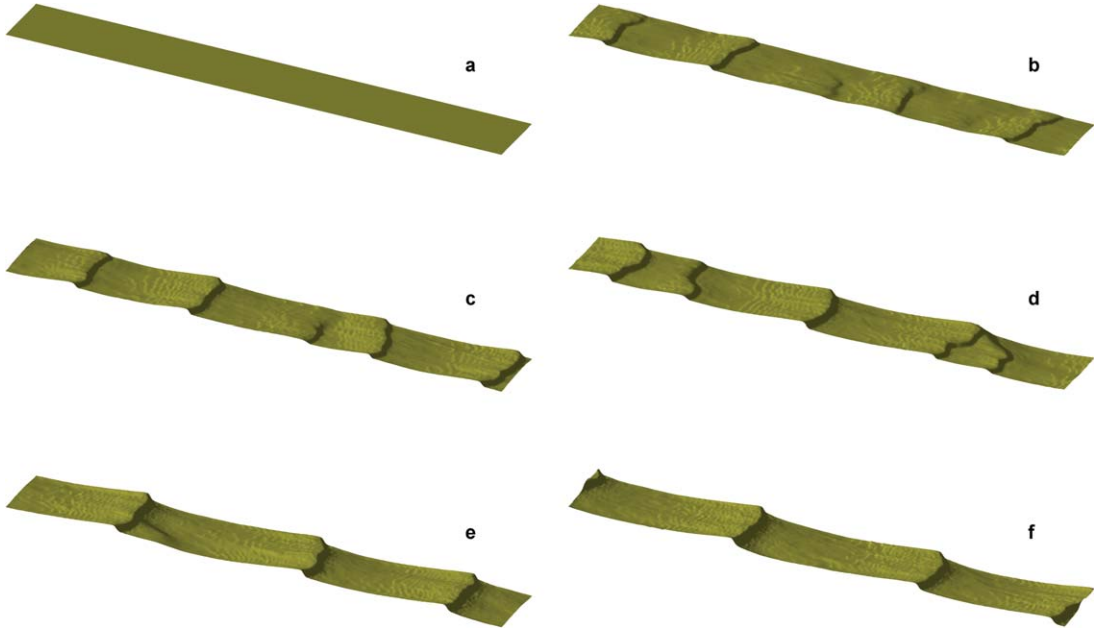

Figure 3. Bed form evolution simulated by numerical model for run RT39. (a) The bed begins from a flat bed, (b) later ripples appear. These ripples grow in size and (c) the dunes begin its formation. (d) These dunes are merged and (e) larger dunes in both length and height are formed. Finally, (f) the bed forms reach their steady state and migrate in the form of two-dimensional dunes.

topographies and making a comparison between these runs unreliable.

[29] The simulated results may have been affected by the imposed periodicity of the boundary conditions, which forces an integer number of dunes in the domain. To avoid this, we imposed separate inflow and outflow boundary conditions in streamwise direction, but we found this did not change the results significantly.

[30] There is a fundamental difference between the change in dune length and dune height. The change in height is related to individual dunes, whereas a change in length is related to the number of dunes on a certain stretch. This may involve higher and lower dunes superimposed onto one another. As the migration speed increases with decreasing dune height [*Niemann et al*., 2011], lower, faster moving dunes move over the stoss side of the higher dunes. When they reach the crest, they merge with the higher dune and form a still larger dune. The sudden changes in height and length of dunes in Figures 5 and 6 are attributed to this merging effect. This complicated phenomenon is enhanced by the presence of the side walls. Somehow, the secondary flow generated by the sidewalls complicates the bed form structure and initially generates dunes of different size. The present averaging procedure for dune height and length, involving different longitudinal bed profiles (not only the one in the centerline), includes the sidewall effect in Figures 5 and 6.

[31] The temporal behavior of the two-dimensional intersections along the centerlines of the bed forms are shown in Figure 7. This figure shows the centerline bed profile for runs RT11, RT39 and the experimental bed profile measurement of T11 associated with run RT11. Phenomena such as splitting and merging clearly emerge from this figure, for the current simulations and experimentally measured profiles. Case RT11 yields three-dimensional dunes, whence the dunes in the centerline are not necessarily of constant size. The dunes in case RT39 are nearly two-dimensional and they approach nearly constant dimensions.

[32] The turbulent coherent structure is a main factor in sediment transport and hence in the generation, growth, and migration of dunes. The sediment transport is significantly affected by the turbulent fluctuations generated in the vicinity of the bed. The turbulence structures are also affected by the topography of the bed, which yields a fully coupled process in morphodynamical problems. The bed starts to deform at small scales as a result of turbulence fluctuations close to the bed. Figure 8 shows the initial deformation under the turbulent structures. The coherent structures are visualized by plotting the iso-surface of the Q

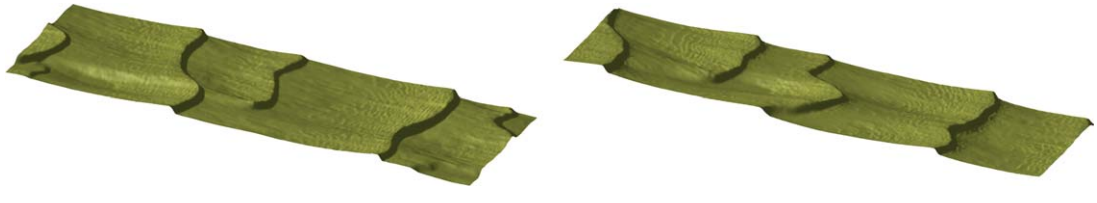

Figure 4. Instantaneous bed form geometry after steady state simulated by numerical model for runs RT01 (left) and RT31 (right).

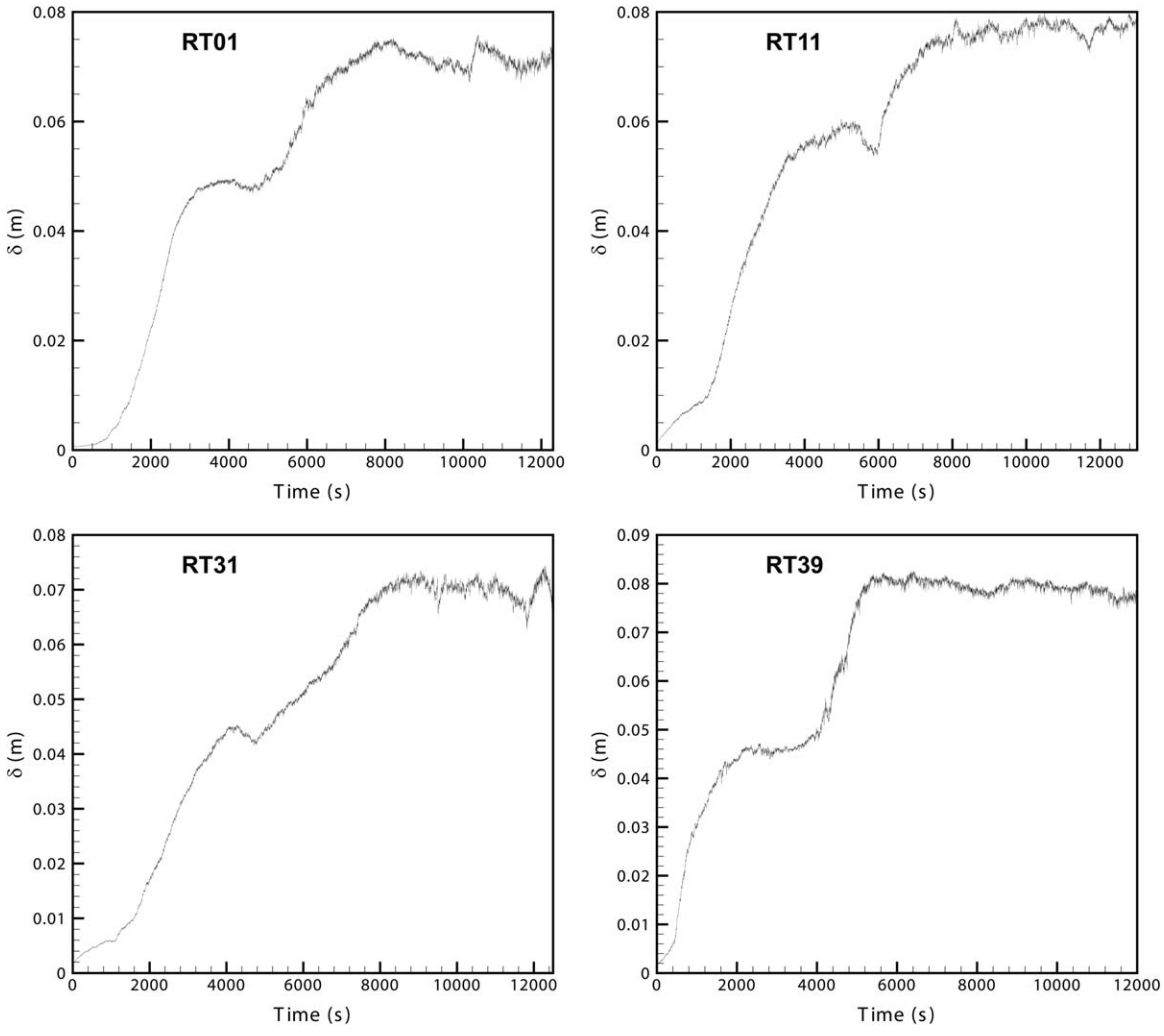

Figure 5. The evolution of mean dune height versus time for runs RT01 to RT39.

function proposed by *Hunt et al*. [1988] and discussed in *Nabi et al*. [2012b]. A value of $Q = 40\ \mathrm{s}^{-2}$ has been selected, which means that the small-scale eddies (smaller than for $Q = 40\ \mathrm{s}^{-2}$) are filtered out. Figure 8a shows that the large structures are almost absent. The initial deformation of the bed forms starts under small eddies, namely by fluctuating bed shear stress.

[33] This deformation is associated with reforming the flow structure and the flow structure, in its turn, affects the sediment transport differently, which creates a fully unsteady coupled process. Such kind of action continues and the deformation of the bed increases in amplitude because of unsteadiness in the erosion and deposition of sediment. The small-scale deformations are superimposed and form relatively larger structures (ripples). As the ripples have more effect on the flow, larger turbulent structures are generated behind the ripples as shown in Figure 8b, most probably through the formation of small recirculation zones in the lee side of the ripples. They are horseshoe-type vortices as discussed in *Nabi et al*. [2012b]. The horseshoe vortices affect the sediment transport significantly [*Grigoriadis et al*., 2009] and yield a significant deformation in the bed. As the ripples increase in size, the flow structure is affected more strongly, the turbulent structures become larger, and the bed deforms faster (Figure 8c). This process increases the size of the ripples by merging and superimposition, and introduces the generation of dunes (Figure 8d). As the dunes are larger in size, they enlarge the horseshoe vortices, increase the sediment transport rate, and increase the dune height, until the process reaches a steady state (Figures 8e and 8f).

[34] Figure 9 shows the turbulent kinetic energy (TKE) above the dunes of run RT11 for two snapshots at 2000 and 5000 s, respectively. As the deformation rate of the bed forms is much smaller than the flow velocity, the flow can be considered as quasisteady. Hence, we selected the bed forms from the solution for the aforementioned time steps and solved the flow on fixed beds, to provide the time averaged values for TKE. Figure 9 shows that the TKE has its maximum behind the dune crests as it was also observed in *Nabi et al*. [2012b], in agreement with the observations of *Grigoriadis et al*. [2009]. The TKE in Figure 9a is associated with the bed forms before they reached their equilibrium. Comparing Figures 9a and 9b shows that the TKE in Figure 9a is smaller because of the lower dunes. The TKE can be observed to increase with increasing dune height. Similar to turbulent coherent structures, TKE forms a coupled mechanism with the bed form.

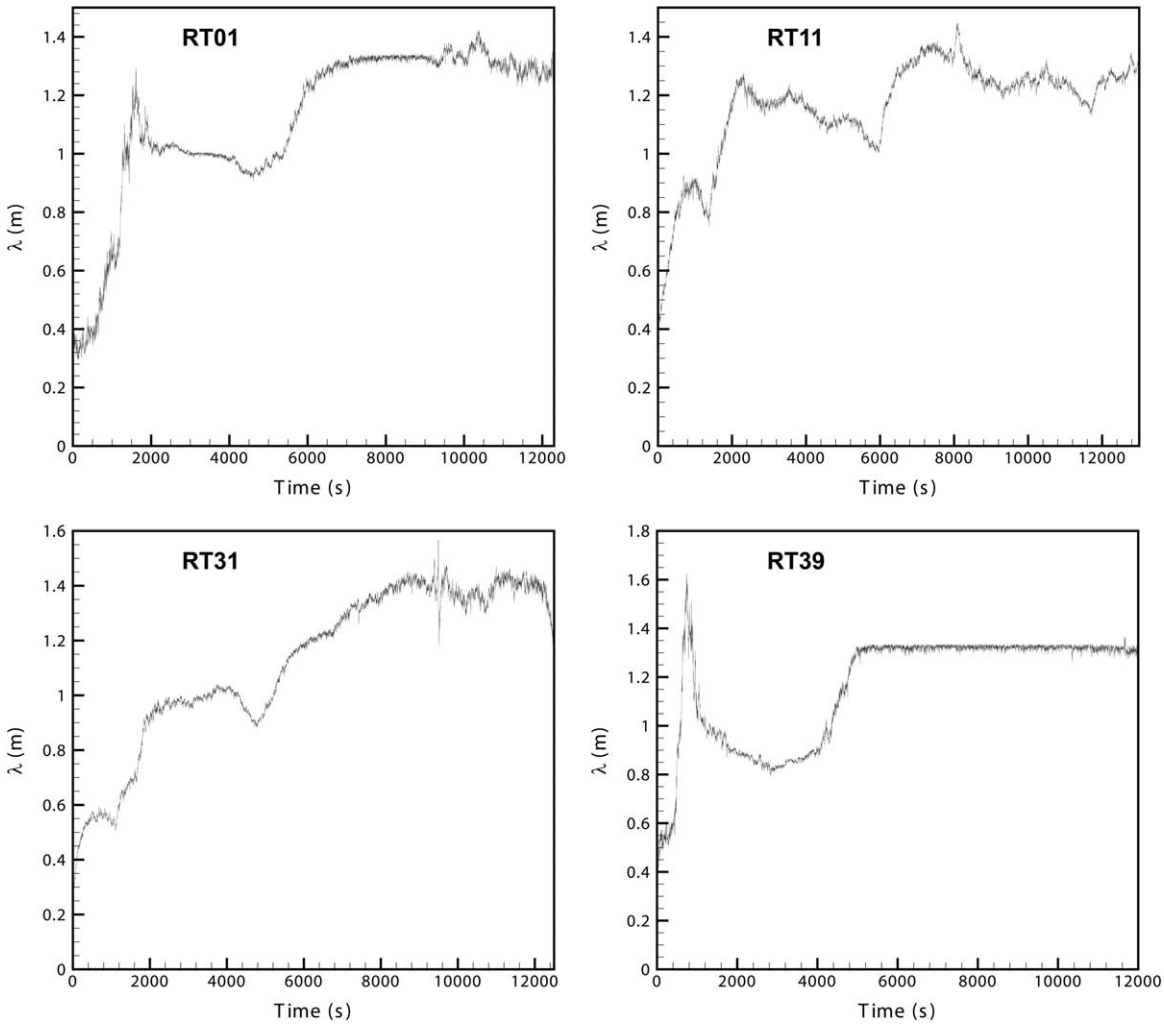

Figure 6. The evolution of mean dune length versus time for runs RT01 to RT39.

[35] The evolution and migration of dunes are governed by sediment transport. In order to visualize this, the sediment particles above the dunes are shown in Figure 10 for run RT01. The concentration of sediment is highest close to the bed. Behind the sharp crests of the relatively high dunes, the sediment forms a kind of cloud, associated with the high-vorticity coherent structure separating from the dune crests and moving up to the water surface. These macroturbulent events are known to be a dominant mechanism for the suspension of sediment over dune beds [*Jackson*, 1976; *Lapointe*, 1992; *Venditti and Bennett*, 2000; *Best*, 2005]. In runs RT11, RT31, and RT39, the same phenomenon is observed.

Table 3. The Mean Dune Shape in an Equilibrium State During Experiment, the Simulations, and the Percentage of Error Between Numerical and Experimental Results

Experiment		T01	T11	T31	T39	C01
	Av. dune height (m)	0.068	0.081	0.068	0.092	0.026
	Av. dune length (m)	1.270	1.194	1.183	1.284	0.305
Simulation		RT01	RT11	RT31	RT39	RC01
	Av. dune height (m)	0.071	0.077	0.070	0.081	0.028
	Av. dune length (m)	1.300	1.240	1.390	1.330	0.330
	Av. migration rate (mm/s)	0.294	0.330	0.383	0.544	–
Error	Av. dune height (%)	4.4	−4.9	2.9	−12	7.7
	Av. dune length (%)	2.4	3.9	17	3.6	8.2

3.2. Effect of Sediment Grain Size

[36] In all experiments, mentioned above, the sediment size was constant. In order to investigate the effect of the sediment diameter on bed topography, different cases were simulated, all with the same flow conditions and domain geometry but different grain size. As the small structures of bed morphology scale with the grain size, the effect of the grain size on the rippled bed can be more obvious. Hence, we selected conditions in which the morphodynamic features fall inside the ripple regime in the phase diagram. At the first stage, we validate the model with an experiment in which the small bed structures dominate.

[37] A series of flume experiments has been carried out at Delft University of Technology [*Crosato et al.*, 2011], in which the small-scale bed forms (ripples) dominate. Although these experiments were mainly meant to investigate the formation of steady bars in a straight channel, bed form dimensions were measured and made available to validate the present numerical model [*Crosato et al.*, 2011].

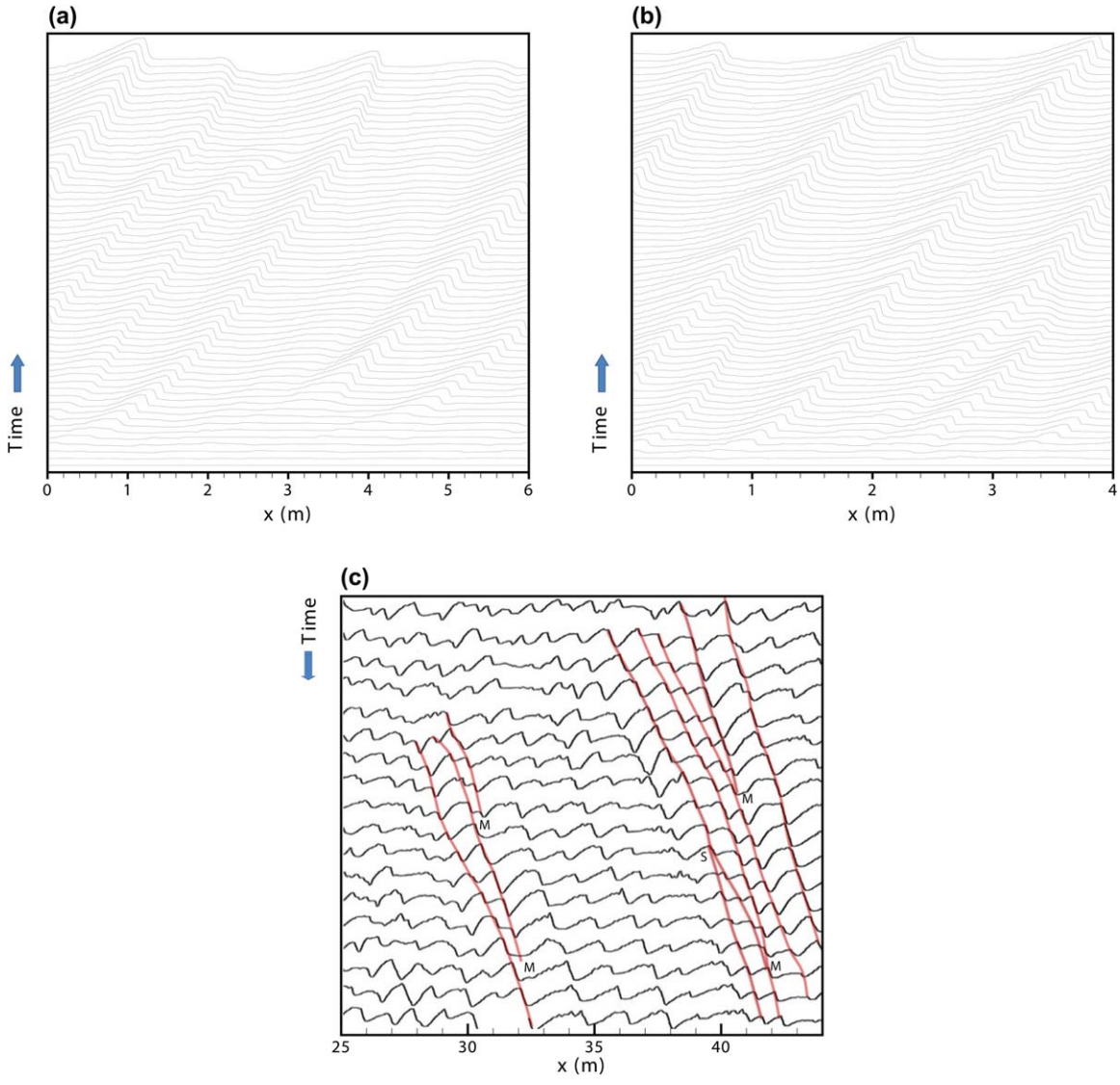

Figure 7. Visualization of evolution of the two-dimensional intersections along the centerlines of the bed forms for (a) run RT11, (b) run RT39, and (c) the experimental measured profile associated with run RT11.

At the first stage, we simulated the case with the same sediment size of Crosato's experiment. The total length of the flume was 25 m, its width 60 cm, and its slope 3×10^{-4}. The bottom of the flume was covered with a 20 cm thick layer of sediment of 0.245 mm median diameter. The experiments started from a flat bed, with a water depth of 4.5 cm, and a discharge of 6.8 L/s. The experimental conditions are given in Table 1.

[38] For the first simulation, the geometrical configurations were selected equal to those in the experimental flume, except the length which was chosen to cover only a 1.2 m long part of the flume (Table 2). The upstream and downstream boundary conditions were taken periodic. The lateral boundaries were taken as smooth solid walls to account for the effect of the glass side walls of the flume. The simulation started from a flat bed, with the same water depth and discharge as in the experiment (Figure 11a). Initially, the bed was perturbed by shear stress fluctuations (Figure 11b), after which ripples were formed (Figure 11c). These ripples grew (Figures 11d and 11e) and finally reached a dynamic equilibrium (Figure 11f). In Figures 11b and 11c, long streamwise ribbon structures can be noticed on the bed. These structures are produced by secondary currents which are generated by the nonhomogeneity and anisotropy of turbulence. Cellular secondary currents can occur in wide open channels and lead to erode the bed cyclically in spanwise direction [*Nezu and Nakagawa*, 1993]. Using a low-pass filter for both measured and simulated bed forms, the mean length and height of the ripples according to the model, 33 cm and 28 mm, respectively (Table 3), agree well with the experimental results (30.5 cm and 26 mm, respectively).

[39] Subsequently, some additional numerical experiments were carried out under similar flow conditions but for finer grain sizes, namely 100, 120, 140, 160, 180, 200, and 200 μm. The results are depicted in Figure 12 for each grain size, from which it can be seen that all simulations with finer sediment yielded ripple-like bed forms. This

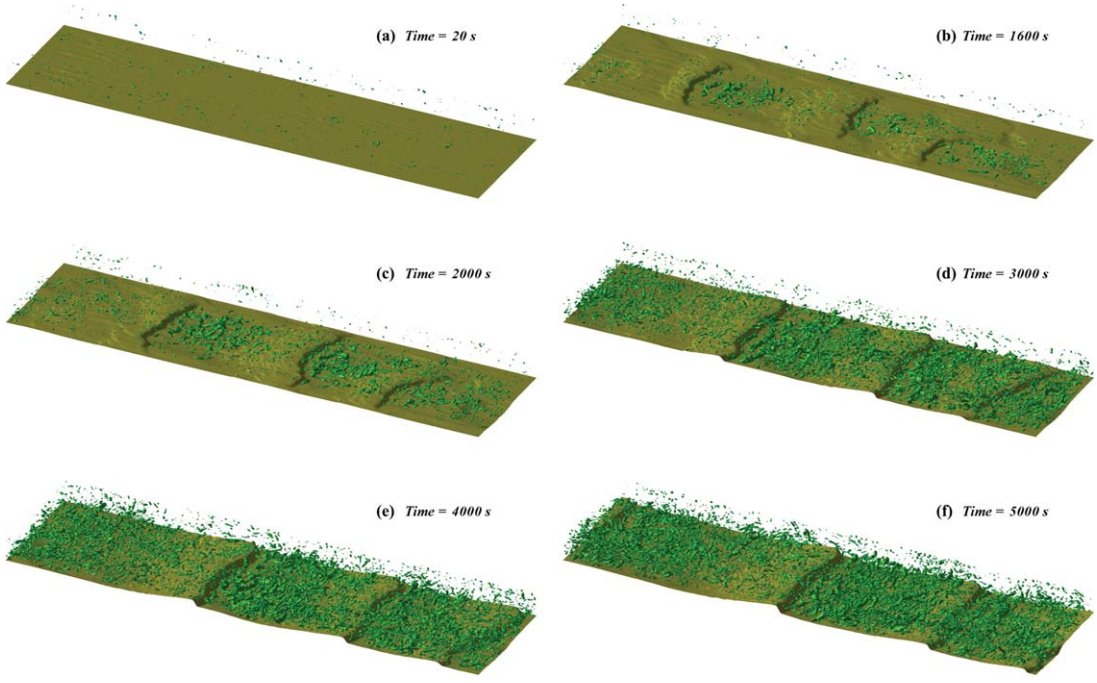

Figure 8. The turbulence coherent structures above the bed forms for run RT11 with $Q = 40\ s^{-2}$. (a) The initiation of the bed deformation, (b) generation of horseshoe vortices by the ripples, (c) increasing the deformation of the bed, (d) increasing the size of horseshoe vortices and the generation of dunes, (e) increasing the height of dunes by large horseshoe vortices, and (f) the bed reaches equilibrium.

phenomenon can be explained by the bed form phase diagram of *Southard and Boguchwal* [1990]. All numerical experiments fell in the ripple regime given the grain sizes and the bulk velocities. The numerical mode reproduced this properly. The finer the sediment (under the same flow conditions), the closer were the bed forms to a two-dimensional shape. Bed forms developed a more irregular shape at larger grain sizes. This could not be derived from Crosatos experiment (Figure 11). Moreover, the finer the sediment, the more superimposed ripples can be observed (i.e., Figures 12a–12d)

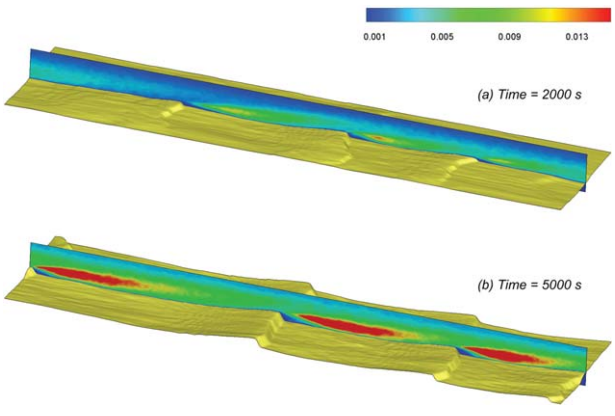

Figure 9. The turbulence kinetic energy above the bed on the centerline intersection of run RT11 after (a) 2000 s and (b) 5000 s. The maximum turbulent kinetic energy is located behind the crest. The turbulent kinetic energy increases with increasing the bed amplitudes.

3.3. Local Scour Around a Circular Pier

[40] The focus of *Nabi et al*. [2012b, 2013] and the present paper is on subaqueous ripples and dunes, but full verification of the 3-D performance of the model is hampered by a lack of experimental measurements for three-dimensional ripples and dunes. We therefore simulated the morphological evolution of scour around a pier, which has a more pronounced 3-D character. We compared the model results with experimental results from *Khosronejad et al*. [2012].

[41] *Khosronejad et al*. [2012] studied experimentally the morphological change of a sand bed in a straight rectangular flume with piers mounted vertically on the bed and centered along the channel centerplane. They used three different pier shapes: cylindrical, diamond-shaped, and square-shaped. The flume was 10 m long, 1.21 m wide, and 45 cm deep, and contained a 20 cm deep layer of uniformly graded noncohesive fine sand material with a mean particle diameter of $d_{50} = 0.85$ mm. The piers were mounted on the bed at 4 m downstream of the channel inlet. All rigid walls

Figure 10. Visualization of the sediment particles above the bed forms for run RT01. The concentration of sediment is highest behind the crest of sharp dunes, due to the boiling effect.

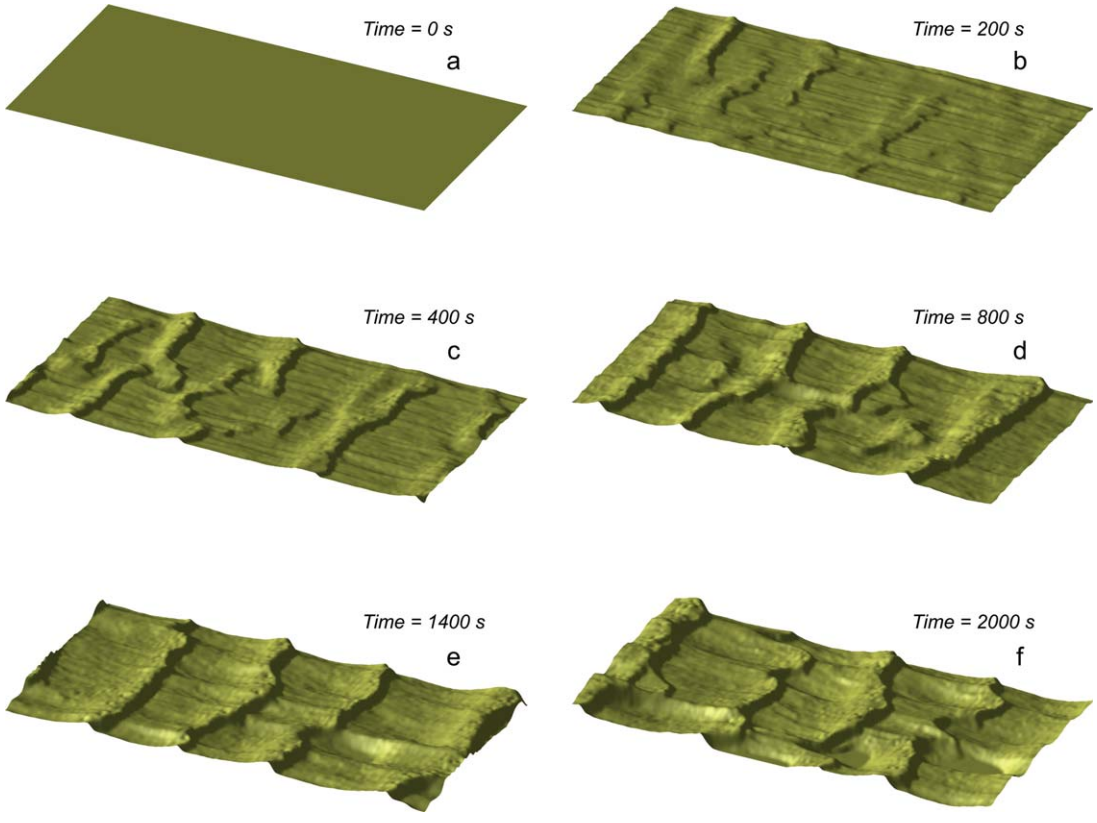

Figure 11. Simulation of evolution and migration of ripples and dunes with sediment diameter of 245 μm.

including the pier surface and flume side walls were hydraulically smooth. For the cylindrical shape, the experiment was run with a bulk inflow velocity of 0.25 m/s corresponding to a uniform flow depth of 18.6 cm with a corresponding Reynolds number of $Re = 46{,}000$ and a Froude number of $Fr = 0.18$. The diameter of the cylindrical pier was 16.51 cm.

[42] We selected the cylindrical pier as a validation case for our model. The conditions for the simulation were chosen identical to the experimental conditions. The simulation started from a flat bed with a morphology factor of 10. The simulation was run until an equilibrium condition of the bed was achieved. The equilibrium condition is assumed to be reached when the rate of increase of scour depth does not exceed 5% of the pier diameter over a period of 12 h [*Khosronejad et al*., 2012].

[43] Figure 13 shows the instantaneous elevation of the bed around the cylinder. The erosion starts from the sides of the cylinder making an angle with the symmetry plane (Figure 13a). This angle is associated with the "recurrent ejection events" as it is mentioned in *Escauriaza and Sotiropoulos* [2011]. During such an event, groups of sediment grains are lifted and travel faster than the other particles at the same time. They also showed that these events initially occur at an angle of 40° from the symmetry plane, which is consistent with our computed results. In a later stage, the energetic turbulent horseshoe vortices dominate and start to erode the bed from the front side of the cylinder (Figure 13b). The turbulent horseshoe vortices continue the erosion process and form a hole in the upstream part around the cylinder, and a deposition part behind the cylinder, because of weak flow in the region behind the cylinder (Figure 13c). The scour depth and the deposited parts increase in size and finally reach an equilibrium, after which no further increase in scour depth and deposition height can be observed (Figure 13d).

[44] In Figure 14, we compare the computed equilibrium bed topography with the laboratory measurements conducted by *Khosronejad et al*. [2012]. A number of important observations can be derived from this figure. The maximum calculated scour depth falls at the upstream side, and the maximum deposition height falls at the downstream side of the pier. It agrees well with the observations of *Khosronejad et al*. [2012] and previous studies by *Dargahi* [1990]. The computed maximum scour depth at an angle of approximately 40° from the symmetry plane is consistent with the experimental results of *Khosronejad et al*. [2012] and *Dargahi* [1990]. The bed elevation contours at the upstream side of the cylinder shows a good agreement with the experimental results. However, a considerable difference can be observed in the deposition part behind the cylinder. This can be explained from the occurrence of von Kármán Street vortices behind the cylinder, which cause temporal variations in the bed morphodynamics. Although the maximum depth and height may reach a statistically equilibrium state, the location and the shape of the bed profiles change in time (dynamic equilibrium). The dynamic equilibrium can also be observed in the migration of dunes as they become affected by complex turbulence structures such as recirculation zones and shear layers.

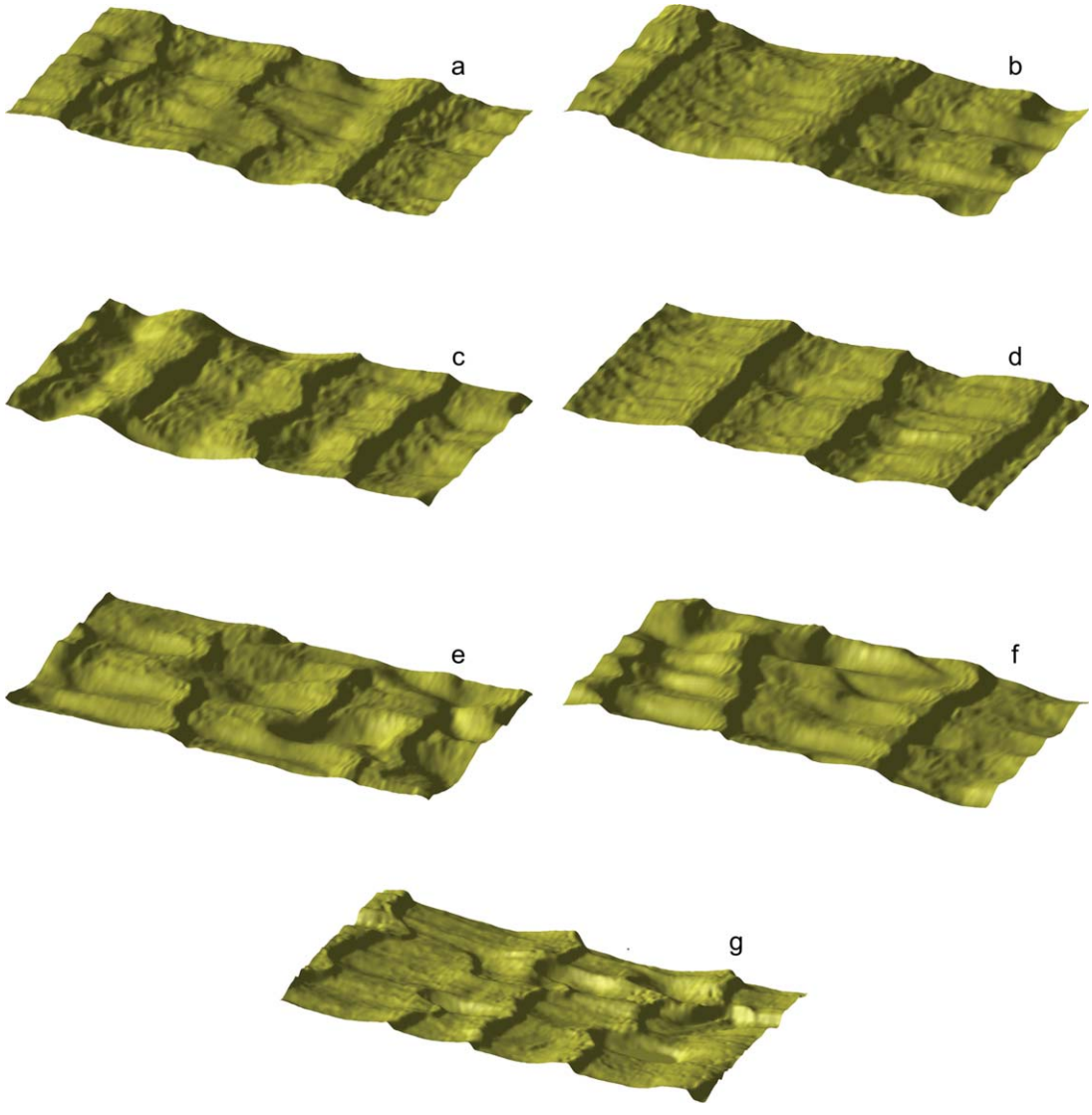

Figure 12. Simulation of bed forms for different sediment diameters. (a) 100 μm, (b) 120 μm (c) 140 μm, (d) 160 μm, (e) 180 μm, (f) 200 μm, and (g) 220 μm.

[45] The calculated time evolution of the maximum scour depth is compared with the experimental results provided by *Khosronejad et al*. [2012] in Figure 15. This Figure 15 shows the computed scour evolution to be in good agreement with the measurements for the first 50 min, for which experimental data are available. However, the rate of erosion in the computed results for the first 5 min is faster than in the experimental measurements. This computed rapid erosion can be attributed to the different mechanisms that appear to drive the scouring process at early times. During the first few minutes of the process, scour occurs at the sides of the pier (at angles of 40°) driven by the increase in the local bed shear stress above the critical value due to the acceleration of flow as it is directed around the pier. At later times, the turbulent horseshoe vortices grow and begin to dominate and affect the dynamics of scour at the front part of the cylinder [*Dargahi*, 1990; *Khosronejad et al*., 2012]. As discussed in *Nabi et al*. [2012b], the present LES model employs a wall function close to the bed which may affect the velocity profile, as well as the bed shear stress, in the regions with complex geometries in which recirculation or rapid acceleration occurs. This leads to an overprediction of the shear stress and the associated rapid erosion at the early times of scouring. However, in the later stage, as the horseshoe vortices dominate, the computed scour depth shows a good agreement with the experimental results.

4. Conclusions

[46] In this paper and two companion papers [*Nabi et al*., 2012b, 2013], we presented a model to simulate the evolution of subaqueous ripples and dunes on the basis of detailed 3-D process descriptions of turbulent flow and sediment transport. The turbulent flow is modeled by LES on a Cartesian grid with local refinements, which gives relatively accurate results while being computationally efficient.

[47] We employ a sophisticated method for sediment transport based on particle techniques. The bed morphology is derived from the sediment model by keeping track of sediment pickup and deposition as sources and sinks in

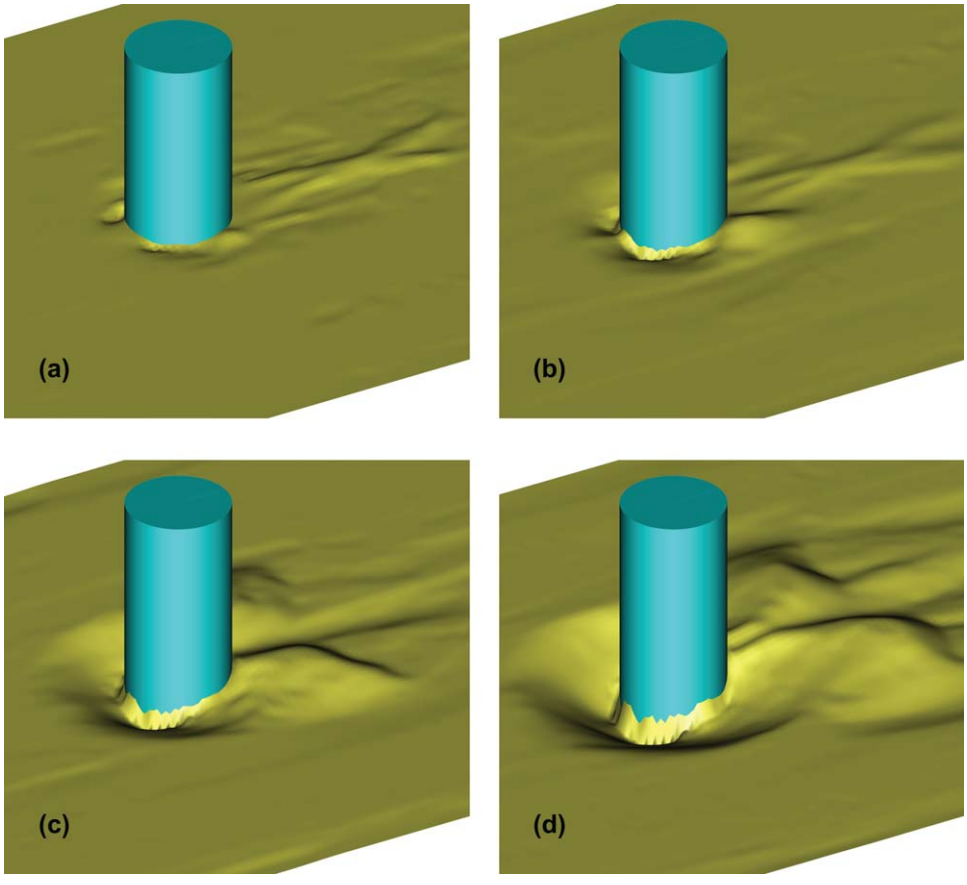

Figure 13. Three-dimensional instantaneous images of the bed elevation, showing the evolution of the scour hole at time (a) 10 s, (b) 100 s, (c) 1000 s, and (d) 3000 s.

each cell, and by taking sediment transport over the bed into account.

[48] In order to validate our model, we simulated four laboratory experiments from *Bakker et al*. [1986] and one laboratory experiment from *Crosato et al*. [2011]. The model results were found to agree well with the experimental findings. The merging of smaller and larger bed forms was found to yield irregularities in the evolution of dune

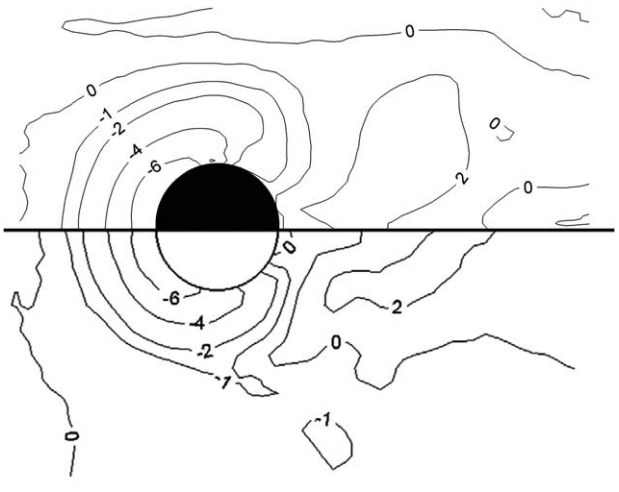

Figure 14. Comparison of (bottom) measured and (top) computed bed topography at equilibrium (in cm). The flow direction is from left to right.

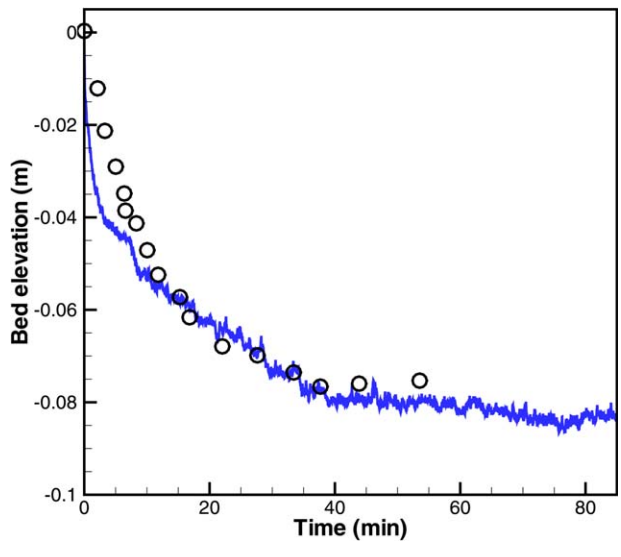

Figure 15. Comparison between the computed and the measured time evolution of the maximum scour depth around the cylindrical pier.

length and height. The effect of coherent turbulence structures on initiation, growth, and migration of dunes was also investigated. It is shown that that bed form development and the generation of turbulence eddies form a coupled process, amplifying each other until the dunes are fully developed and reach a steady state.

[49] When changing the sediment grain size while keeping all other conditions the same, a smaller grain size was found to generate more superimposed ripples. Moreover, the finer sediments were found to yield nearly two-dimensional bed forms. As the sediment size increased, the irregularities on the bed increased.

[50] As an additional verification for pronounced 3-D morphologies, the model was applied to simulate the local scour around piers from a laboratory experiment by *Khosronejad et al*. [2012]. The model generated the scour realistically and reproduced most of the physical phenomena reported in previous studies. The results showed a good agreement with the experiment for both the transient development and the final equilibrium configuration of the bed.

[51] The present model has the potential to constitute a basis for bed roughness and sediment transport parameterization under steady as well as varying flow conditions for use in large-scale morphodynamic models. The physics-based formulation provides a fair level of confidence that application of the model can be extended to rare extreme events [*Nabi et al*., 2012a]. Such applications are needed if flood protection design standards are based on return periods of centuries or millennia.

[52] **Acknowledgments.** The work presented herein was carried out as part of the work package "River Morphology" of Delft Cluster project 4.30 "Safety against flooding," financed by the Netherlands government and supported by Rijkswaterstaat Waterdienst. The authors are grateful to Sanjay Giri for his fruitful suggestions and to Alessandra Crosato for providing the data from the flume experiment of *Crosato et al*. [2011].

References

Ashley, G. M. (1990), Classification of large-scale subaqueous bedforms: A new look at an old problem, *J. Sediment. Petrol.*, *60*, 160–172.

Bakker, B., A. J. Struijk, and H. Nijdam (1986), Flume experiments on dunes under steady flow conditions (uniform sand, Dm = 0.77 mm), description of bed forms, technical report, vols. 1–3, TOW rivers R 657-XIX/M 1314 part VIII, WL—Delft Hydraul., Delft, Netherlands.

Best, J. (2005), The fluid dynamics of river dunes: A review and some future research directions, *J. Geophys. Res.*, *110*, F04S02, doi:10.1029/2004JF000218.

Crosato, A., E. Mosselman, F. B. Desta, and W. S. J. Uijttewaal (2011), Experimental and numerical evidence for intrinsic nonmigrating bars in alluvial channels, *Water Resour. Res.*, *47*, W03511, doi:10.1029/2010WR009714.

Dargahi, B. (1990), Controlling mechanism of local scouring, *J. Hydraul. Eng.*, *116*(10), 1197–1214.

Engelund, F. (1970), Instability of erodible beds, *J. Fluid Mech.*, *42*(2), 225–244.

Escauriaza, C., and F. Sotiropoulos (2011), Lagrangian model of bed-load transport in turbulent junction flows, *J. Fluid Mech.*, *666*, 36–76.

Fredsøe, J. (1982), Shape and dimensions of stationary dunes in rivers, *J. Hydraul. Div. Am. Soc. Civ. Eng.*, *108*(8), 932–947.

Giri, S., and Y. Shimizu (2006), Numerical computation of sand dune migration with free surface flow, *Water Resour. Res.*, *42*, W10422, doi:10.1029/2005WR004588.

Grigoriadis, D. G. E., E. Balaras, and A. A. Dimas (2009), Large-eddy simulations of unidirectional water flow over dunes, *J. Geophys. Res.*, *114*, F02022, doi:10.1029/2008JF001014.

Guy, H. P., D. B. Simons, and E. V. Richardson (1966), Summary of alluvial channel data from flume experiments, 1956–1961, *U.S. Geol. Surv. Prof. Pap.*, *462-I*, 1–96.

Hunt, J. C. R., A. A. Wray, and P. Moin (1988), Eddies, streams and convergence zones in turbulent flows, in *CTR Annual Research Briefs NASA Ames*, Stanford Univ. Press, Stanford, Calif.

Jackson, R. G. (1976), Sedimentological and fluid dynamic implications of the turbulence bursting phenomenon in geophysical flows, *J. Fluid Mech.*, *77*, 531–560.

Kennedy, J. F. (1963), The mechanics of dunes and antidunes in erodible-bed channels, *J. Fluid Mech.*, *16*, 521–544.

Khosronejad, A., S. Kang, and F. Sotiropoulos (2012), Experimental and computational investigation of local scour around bridge piers, *Adv. Water Resour.*, *37*, 73–85.

Kraft, S., W. Yongqi, and M. Oberlack (2011), Large eddy simulation of sediment deformation in a turbulent flow by means of level-set method, *J. Hydraul. Eng.*, *137*(11), 1394–1405.

Lapointe, M. (1992), Burst-like sediment suspension events in a sand bed river, *Earth Surf. Processes Landforms*, *17*, 253–270.

Nabi, M. (2012a), Computational modelling of small-scale river morphodynamics, PhD thesis, Delft Univ. of Technol., Delft, Netherlands.

Nabi, M., H. J. de Vriend, E. Mosselman, C. J. Sloff, and Y. Shimizu (2012b), Detailed simulation of morphodynamics: 1. Hydrodynamics model, *Water Resour. Res.*, *48*, W12523, doi:10.1029/2012WR011911.

Nabi, M., H. J. de Vriend, E. Mosselman, C. J. Sloff, and Y. Shimizu (2013), Detailed simulation of morphodynamics: 2. Sediment pick-up, transport and deposition, *Water Resour. Res.*, doi:10.1002/wrcr.20303, in press.

Nelson, J. M., R. L. Shreve, S. R. McLean, and T. G. Drake (1995), Role of nearbed turbulence structure in bed load transport and bed form mechanics, *Water Resour. Res.*, *31*(8), 2021–2086.

Nezu, I., and H. Nakagawa (1993), *Turbulence in Open-Channel Flows*, A. A. Balkema, Rotterdam, Netherlands.

Niemann, S. L., J. Fredsøe, and N. G. Jacobsen (2011), Sand dunes in steady flow at low Froude numbers: Dune height evolution and flow resistance, *J. Hydraul. Eng.*, *137*(1), 5–14, doi:10.1061/(ASCE)HY.1943–7900.0000255.

Paarlberg, A. J., C. M. Dohmen-Janssen, S. J. M. H. Hulscher, and P. Termes (2009), Modeling river dune evolution using a parameterization of flow separation, *J. Geophys. Res.*, *114*, F01014, doi:10.1029/2007JF000910.

Richards, K. J. (1980), The formation of ripples and dunes on an erodible bed, *J. Fluid Mech.*, *99*(3), 597–618.

Shimizu, Y., S. Giri, S. Yamaguchi, and J. Nelson (2009), Numerical simulation of dune-flat bed transition and stage-discharge relationship with hysteresis effect, *Water Resour. Res.*, *45*, W04429, doi:10.1029/2008WR006830.

Simons, D. B., and E. V. Richardson (1966), Resistance to flow in alluvial channels, *U.S. Geol. Surv. Prof. Pap.*, *422-J*, 1–61.

Simons, D. B., E. V. Richardson, and M. L. Albertson (1961), Flume studies using medium sand (0.45 mm), *U.S. Geol. Surv. Prof. Pap.*, *1498-A*, 1–76.

Southard, J. B., and L. A. Boguchwal (1990), Bed configurations in steady unidirectional water flow part 2. Synthesis of flume data, *J. Sediment. Petrol.*, *60*, 658–679.

Sumer, B. M., and M. Bakioglu (1984), Formation of ripples on an erodible bed, *J. Fluid Mech.*, *144*, 177–190.

Tjerry, S., and J. Fredsøe (2005), Calculation of dune morphology, *J. Geophys. Res.*, *110*, F04013, doi:10.1029/2004JF000171.

Tuijnder, A. P., J. S. Ribberink, and S. J. M. H. Hulscher (2009), An experimental study into the geometry of supply-limited dunes, *Sedimentology*, *56*, 1713–1727.

Van der Mark, C. F., A. Blom, and S. J. M. H. Hulscher (2008), Quantification of variability in bedform geometry, *J. Geophys. Res.*, *113*, F03020, doi:10.1029/2007JF000940.

Venditti, J. G. (2007), Turbulent flow and drag over fixed two-and three-dimensional dunes, *J. Geophys. Res.*, *112*, F04008, doi:10.1029/2006JF000650.

Venditti, J. G., and S. J. Bennett (2000), Spectral analysis of turbulent flow and suspended sediment transport over dunes, *J. Geophys. Res.*, *105*(C9), 22,035–22,047, doi:10.1029/2000JC900094.

Venditti, J. G., M. Church, and S. J. Bennett (2005), Morphodynamics of small-scale superimposed sand waves over migrating dune bed forms, *Water Resour. Res.*, *41*, W10423, doi:10.1029/2004WR003461.

Wilbers, A. W. E. (2004), The development and hydraulic roughness of subaqueous dunes, PhD thesis, Utrecht Univ., Utrecht, Netherlands.

Zedler, E. A., and R. L. Street (2001), Large-eddy simulation of transport: Currents over ripples, *J. Hydraul. Eng.*, *127*, 444–452.